

Correlated atomic motion and spin-ordering in bcc ^3He

N. Gov ¹ and E. Polturak ²

¹*Department of Physics, University of Illinois at Urbana-Champaign,
1110 Green St., Urbana 61801, IL, USA*

²*Physics Department, Technion-Israel Institute of Technology,
Haifa 32000, Israel*

We propose a new way to treat the ordering of nuclear magnetism of solid ^3He . We argue that the magnetic interaction arises indirectly as a consequence of correlated zero-point motion of the ions. This motion lowers the energy of the ground state, and results in a coherent state of oscillating electric dipoles. Distortion of the electronic wavefunctions leads to hyperfine magnetic interactions with the nuclear spin. Our model describes both the modification of the phonon spectra, localized modes ("vacancies") and the nuclear magnetic ordering of bcc ^3He using a single parameter, the dipolar interaction energy E_0 . The model yields correctly both the u2d2 symmetry of the ordered phase and the volume dependence of the magnetic interaction. We calculate the magnetic excitations in the u2d2 phase, which compare well with the measured specific-heat, free energy and entropy. We further give a description of the nature of the High-Field phase and the phase-transition lines as a function of magnetic field and volume.

PACS: 67.80.-s, 67.80.Jd, 67.80.Cx

I. INTRODUCTION

The spin-ordered phase of bcc ^3He presents a difficult challenge to accurate theoretical description^{1,2}. The main problem is to explain why the transition temperature³ of 10^{-3}K is two orders of magnitude larger than the nuclear dipolar interaction $\sim 10^{-8}\text{K}$. The prevalent description is in terms of atomic exchange cycles involving several atoms (Multiple Spin Exchange model). Successively higher order cycles produce competing ferro and antiferromagnetic interactions⁴. For qualitative description within this Multiple Spin Exchange model (MSE), one needs up to six or more atoms exchanging places, which becomes difficult to calculate and seems a priori less probable^{1,5}. In fact, it is not sure that this description converges^{2,6-8} for larger exchange cycles, i.e. may not be the spin-ordering mechanism. This conceptual problem, despite the relative successes of the MSE picture⁹, therefore raises the interest in another approach¹⁰.

We propose that magnetic ordering of ^3He is a result of correlations in the zero point atomic motion, which however does not require exchange of atoms¹¹. These correlations lower the energy of the ground state¹² and result in a coherent state of oscillating electric dipoles, which also modify the phonon spectrum. We show here that the zero-point motion of the atoms produces an oscillating magnetic polarization of the electronic cloud which interacts with the nuclear spin in each atom. The nuclear spins interact with each other indirectly, through the electric dipolar interaction between the atoms. In effect, this interaction is hyper-fine like, and has the right order of magnitude to be related to the spin-ordering transition. In addition, we show that the volume dependence of the on-site magnetic interaction is in agreement with experimental data, and that the space symmetry of

the proposed interaction leads naturally to the distinct u2d2 antiferromagnetic phase. Our scenario is somewhat similar to the mechanism of hyperfine enhanced nuclear magnetism that occurs in certain insulators¹³.

The plan of the paper is as follows: In section II we establish the applicability of our model of zero-point electric dipoles in bcc ^3He . In section III we describe the hyperfine magnetic interactions and their volume dependence. In section IV we show how the indirect dipolar interactions induced by the on-site hyperfine interactions lead to the u2d2 symmetry of the ordered phase. In section V we calculate some properties of the u2d2 phase and compare them to the experimental data. In section VI we give a description of the nature of the high-field phase (HFP) and calculate its properties.

II. COHERENT DIPOLES IN THE BCC GROUND-STATE AND TRANSVERSE PHONONS

At temperatures which are high compared to the magnetic interactions ($T \gg 1\text{mK}$), the atomic motion in bcc ^3He can be treated in the same way as in ^4He ¹¹.

We begin by observing^{11,14} that in contrast to the situation prevailing in gaseous He, the interatomic potential is highly anisotropic in the bcc crystal. The potential well is both very wide and anharmonic (double-well) along the major axes (100,010,001). This means that the atomic wavefunctions will be particularly extended in these directions. In order to reduce the repulsive overlap energy, the many-body wavefunction has to include "dynamic-correlations"¹⁵. The current treatment using variational wavefunction¹⁴ incorporates these correlations using a Jastrow-type wavefunction that has a two-body or higher order terms to represent the short-range hard-core repul-

sion. Using this variational wavefunction, the phonon spectrum is calculated through a Self-Consistent Harmonic (SCH) calculation¹⁴. This gives a satisfactory description of most phonon branches, except for the transverse $T_1(110)$ phonon, which experimentally is found to be much softer than calculated. Introducing cubic terms into the calculation to represent the anharmonicity, softens the calculated phonon spectra overall, which ruins the good agreement with the phonon branches other than $T_1(110)$. This SCH+C method also breaks the self-consistency of the Harmonic procedure and predicts an anomalous upward slope of the lowest transverse T_{110} mode, which is not observed.

We would like to describe the anharmonicity in a different way; we treat the local motion of the atom in its potential well as a "local mode". The harmonic description of the crystal potential misses the low-lying vibration of the atoms due to the shallow (double-well) potential along the major axes, which is the mode responsible for the strong dynamic correlations in the many-body wavefunction. We therefore treat the low-energy local excitation along the major axes, and the harmonic modes as two independent degrees of freedom. The collective motion of the atoms is assumed to be well described by the Self Consistent Harmonic calculation. In this procedure, we take the SCH spectrum from previous works¹⁴, as the approximate harmonic description. The "local modes" can be shown to couple only to the $T_1(110)$ transverse phonon¹¹. The coupling is described in terms of an electric dipolar matrix element, where this zero-point dipole moment arises from a correlated atomic motion along the major axes.

The origin of a zero point electric dipole moment is the highly directional zero point oscillation of the nucleus, which breaks the rotational symmetry of the nuclear position relative to the electronic cloud. Going beyond the Born-Oppenheimer approximation, the electronic wavefunction acquires a p-component in addition to the s-orbital. The first order correction to the electronic energy due to relative nuclear-electronic fluctuations is¹⁶: $\Delta E \simeq (m/M_n)(a/D)E_{sp} \simeq 5\text{K}$, where m is the electron mass, M_n the nuclear mass, $a \simeq 0.25\text{\AA}$ is the Bohr radius, $D \sim 0.8\text{\AA}$ is the spread of the excited nuclear wavefunction, and E_{sp} the excitation energy of the He atom from the s to the p shell. Since the crystalline potential is anisotropic, we can take this zero point motion to be highly directional (i.e. a completely off-diagonal matrix element). We assume that ΔE is the energy associated with the mixing of the s and p electronic levels: $|\psi\rangle \simeq |s\rangle + \lambda|p\rangle$, i.e. $\lambda \sim \sqrt{\Delta E/E_{sp}} \sim 10^{-2}$. This local polarization results in zero-point dipolar interactions between the atoms^{11,12}. Taking these interactions into account, the ground state of the crystal can be lowered by having the nuclear motions correlated with respect to the relative phase of this zero-point oscillatory motion. The dipolar interaction energy E_0 , of the order of ΔE , is the energy we associate with the correlated zero-point

oscillations of the atoms along the major axes.

In our scenario, the ground-state of the crystal in which the zero-point motion of the atoms is correlated may be described as a global state of quantum resonance between the two degenerate configurations shown in Fig.1, each of which minimizes the instantaneous dipolar interaction energy¹¹ for dipoles along the major axes (i.e. $\hat{\mu} = \hat{x}, \hat{y}, \hat{z}$)

$$E_{dip} = - \sum_{i \neq 0} \mu_0 \cdot \mu_i \left[\frac{3 \cos^2(\hat{\mu} \cdot (\mathbf{r}_0 - \mathbf{r}_i)) - 1}{|\mathbf{r}_0 - \mathbf{r}_i|^3} \right] \quad (1)$$

where \mathbf{r}_0 is the position of an atom and the summation \mathbf{r}_i runs over the entire lattice. The atomic electric dipole moment $|\mu|$ induced by the coherent zero-point motion is proportional to λ through

$$|\mu| = e \langle \psi | x | \psi \rangle \simeq 2e\lambda \langle s | x | p \rangle \quad (2)$$

Due to the lower symmetry of the dipolar array (Fig.1) compared to the crystal symmetry, a coupling between the harmonic phonons and the dipolar modulation exists only along the (110) direction¹¹. The excitations of these dipoles are periodic modulations of the relative phases of the dipoles, with respect to the ground state array (Fig.1). We found that the dipolar interactions vanish at the edge of the Brillouin zone, so this transverse phonon has the energy E_0 at this point. The hybridization of the dipolar excitations with the phonons results in a factor 2 softening of the transverse $T_1(110)$ phonon compared to the harmonic calculation. The experimental data give a softening by a factor of ~ 1.7 , in close agreement. In addition, in our model there appears a localized (i.e. dispersionless) excitation branch of energy $2E_0$, which is involved in mass diffusion and contributes to the specific-heat¹¹. This excitation is a quantum analogue of a point defect ("vacancy") and has similar features¹¹. The specific heat of the localized mode is consistent with the experimental contribution attributed to point defects to the total heat capacity, and in fact resolves previous inconsistencies related to the properties of the point defects in this solid (vacancies)¹⁷. Let us emphasize that the additional modes are a consequence of introducing an additional degree of freedom to the solid¹², which is the relative phase of the internal mixing of the $|s\rangle$ and $|p\rangle$ states.

In the case of bcc ^4He the bare local mode energy E_0 was measured directly by NMR of a ^3He impurity, and the phonon spectrum was measured using neutron scattering. Our calculation is consistent with both sets of data¹¹. There are no neutron scattering measurements of the phonon spectrum of bcc ^3He , but sound velocity data indicates that the slope of the $T_1(110)$ phonon is about half of the SCH calculation^{18,19}. We predict that this ratio should indeed be 1/2, and we therefore take half the energy of the calculated¹⁹ SCH $T_1(110)$ phonon at the edge of the Brillouin zone to be the bare dipole-flip

energy $E_0 (\simeq 5\text{K at } V=21.5\text{cm}^3/\text{mole})$ in solid ^3He . According to our model, the energy of the localized mode involved in thermally activated self-diffusion should be $2E_0 \simeq 10\text{K}$. This value is in excellent agreement with the activation energy measured by x-ray diffraction, ultrasonics and NMR experiments²⁰ at $V=21.5\text{cm}^3/\text{mole}$. A similar activation energy is also obtained from the excess specific heat²¹, and pressure measurements²².

We therefore establish the likely occurrence of coherent zero-point dipoles in the ground-state of bcc ^3He . The volume dependence of the dipolar energy (i.e. the 'vacancy' activation energy $2E_0$) is shown in Fig.2a from various experimental sources^{20,18}. Since the excitation energy of the atom inside the crystal potential increases with decreasing volume, we indeed expect the energy $2E_0$ to behave as in Fig.2a. The mixing parameter λ depends on pressure through $\sqrt{VE_0}$, where V is the molar volume. This behavior arises from the definition of E_{dip} (1),(2) and the factor $|\mathbf{r}_0 - \mathbf{r}_i|^3$ in this equation is proportional to the molar volume V . We plot the result in Fig.2b, where we see that λ increases slowly with decreasing molar volume V . Future x-ray studies²³ in bcc ^3He may be able to check our prediction for the relation between the activation energy ($2E_0$, Fig.2a) and the $T_1(110)$ phonon as a function of the molar volume.

III. MAGNETIC INTERACTIONS

We now describe the magnetic interaction arising within our model. The lowest $|p\rangle$ level of the He atom has the electrons in a spin $S = 1$ state due to strong exchange interaction²⁴, of the order of 0.25eV . The zero-point electric dipole interactions, arising from the relaxation of the Born-Oppenheimer approximation, are also accompanied by electronic spin interactions due to magnetic-dipole transitions. The size of the electric dipole matrix is given by the electric dipolar interaction energy $E_0 = 2|E_{dip}|$ (1). The size of the magnetic-dipole matrix is related to the electric dipole matrix by²⁴

$$E_{magtrans} \simeq E_0 \cdot (\hbar/M_a c_s) / \langle x \rangle \quad (3)$$

where M_a is the atomic mass, c_s is the velocity of sound of the T_{110} phonon. We find that $\hbar/mc_s \sim \langle x \rangle \simeq 0.8\text{\AA}$ so that both transition matrices are of the same order. We therefore have oscillating zero-point electric and magnetic dipoles, with an electric dipole moment of size $\sim 2e\lambda\langle x \rangle$ and a magnetic dipole moment of size $\sim 2\lambda n_e$, where n_e is the electron's magnetic moment.

In addition, the atomic p -state, $S = 1$ level is split into 3 sublevels with quantum numbers: $J = L + S = 0, 1, 2$, due to spin-orbit coupling²⁴, which is of the order of $\sim 1.5\text{K}$. In our particular sp -hybridized states, which are not pure states of the quantum number J , there is no spin-orbit coupling, as the orbital current is zero. Rather, these states are split as a consequence of the magnetic

dipolar interaction between the two electrons. The magnetic interaction will tend to align the total electronic spin with the symmetry axis of the excited $|p\rangle$ state, i.e. along the normal axes (Fig.3). This follows from a simple calculation of the magnetic dipolar interaction of the two electrons, in which the $|s\rangle$ electron is centered on average in the nucleus, while the $|p\rangle$ electron is spread over the two lobes (Fig.3). We thus estimate the aligning dipolar interaction energy at $E_{es} \sim 1.4\text{K}$, of the order of the spin-orbit coupling.

In the ground state, the zero-point $|p\rangle$ electrons will therefore have an oscillating magnetic moment $\mathbf{N}_e \sim 2\lambda n_e$, where n_e is the magnetic moment of an electron. Because part of the electronic magnetic moment is now associated with the $|p\rangle$ state, there appears a net uncanceled moment of equal size in the $|s\rangle$ component of the electronic wavefunction. In ^4He the nuclear spin is zero, and the zero-point magnetic polarization of the electrons has no effect. In contrast, in ^3He the nuclear magnetic spin $I = 1/2$ will interact with the oscillating electronic magnetic moment, mainly due to the contact term of the $|s\rangle$ electron at the nucleus. The magnetic interaction is of the hyper-fine type²⁴, and the energy associated with it, E_{mag} , is given by

$$E_{mag} = \left\langle -\frac{8\pi}{3} \mathbf{N}_e \cdot \mathbf{N}_n \delta(r) \right\rangle \quad (4)$$

where \mathbf{N}_n is the effective nuclear magnetic moment, reduced empirically⁵ by a factor of 0.83 due to zero-point fluctuations of the nuclear spins²⁵. Using experimental hyper-fine data²⁶, we find the maximum value of $E_{mag}/k_B \simeq 4.5\text{mK}$ (for $V=24\text{ cm}^3/\text{mole}$). This energy is much larger than the direct nuclear dipole-dipole interaction ($\sim 0.1\mu\text{K}$), and is of the right magnitude to explain the high transition temperature of nuclear ordering in bcc ^3He . A diagram of the energy scales involved in the magnetic interactions is shown in Fig.4, where we show the cascade of the different interactions that ultimately align the electronic and nuclear spins, with the zero-point excitations of the p -state.

Before proceeding to describe the nuclear spin ordering phenomenon, and the effect of the magnetic interactions on the zero-point electric dipoles, we present a quantitative calculation of the volume dependence of the magnetic interaction at $T=0$. It is known empirically that these interactions have a strong volume dependence¹, usually described as: $E_{mag} \propto V^{18}$. In our model, the magnetic energy (4) will change with pressure due to changes of the electronic magnetic polarization \mathbf{N}_e . First, the pressure changes the admixture of the $|p\rangle$ orbital in the ground state wavefunction $|\psi\rangle$, through changes of the mixing parameter λ . Second, as the solid is compressed, the 3 sub-levels ($J = 0, 1, 2$) broaden into partially overlapping bands. This overlap leads to further reduction of the net alignment of the electronic magnetic moment \mathbf{N}_e with the orbital polarization (Fig.3).

The reduction in \mathbf{N}_e due to the broadening of the sub-levels with pressure can be approximated as linearly pro-

portional to the overlap integral of the three spin-orbit sub-levels

$$\langle \mathbf{N}_e(V) \rangle \simeq (1 - F(V)) \lambda(V) \mathbf{N}_e \quad (5)$$

where the overlap integral $F(V) = \int \phi_1^*(E) \phi_{-1}(E) dE$, and $\phi_1^*(E), \phi_{-1}(E)$ are taken as normalized Gaussians centered at the energies of the spin-orbit levels, which are $\sim 1.5\text{K}$ apart²⁴. The effective energy width γ of these Gaussians ($\phi_1^*(E)$ and $\phi_{-1}(E)$) is estimated using a simple band calculation, as the change of the Coulomb energy of the $|p\rangle$ electrons due to overlapping $|p\rangle$ wavefunctions on neighboring He nuclei²⁷

$$\gamma(V) = \lambda^2 \sum_i \int \frac{e^2}{|\mathbf{r}_0 - \mathbf{r}_i|} \psi_0^*(r) \psi_i(r) d^3r \quad (6)$$

where $\psi_0^*(r), \psi_i(r)$ are the p -state wavefunctions of the electrons around the central atom and its i neighbors. In this calculation we also take into account the large spatial spread of the atomic position inside the wide potential well¹¹, of approximately $\pm 0.8\text{\AA}$. We find that γ ranges from $\sim 0\text{K}$ for $V=24\text{ cm}^3/\text{mole}$ to 5.5K for $V=19\text{ cm}^3/\text{mole}$. The overlap factor $1 - F(V)$ is therefore very sensitive to volume, changing from 1 at $V \sim 24.3\text{ cm}^3/\text{mole}$ to ~ 0.01 at $V=19\text{ cm}^3/\text{mole}$. One can see that as the volume decreases the broadening of the bands increases, thereby decreasing the net magnetic polarization of the electronic cloud.

The strength of the magnetic interaction should be proportional to the measured Curie-Weiss temperature θ . In Fig.5 we compare the normalized magnetic interaction energy E_{mag} (4) with the normalized measured¹ θ . We find that the volume dependence of E_{mag} agrees very well with that of θ . Since in our model there is only one magnetic interaction, there is a single energy scale that determines the volume dependence of the transition temperature and the e_2 coefficient of the specific-heat²⁸. All these quantities have the same volume dependence, a simpler situation than that involving a competition among many exchange processes^{1,9}.

IV. COMPOSITE QUANTUM RESONANCE OF THE ELECTRONIC AND MAGNETIC SUBSYSTEMS

We now consider the effects of the magnetic interactions on the coherent-state of the oscillating electronic dipoles. We begin with the high-temperature paramagnetic phase (PP), where the nuclear spins are randomly oriented. The existence of the hyper-fine splitting E_{mag} (4) means that the quantum resonance state of the atoms, oscillating between the two configurations of Fig.1 is broken. The resonance frequency of each site will be slightly different from each other, randomly shifted by $0 - E_{mag}/\hbar$, along each of the 3 major axes. The result will be that the zero-point electric dipoles will slowly drift out of resonance, breaking the long-range order of Fig.1.

It is possible to restore the degeneracy of the overall ground state, and hence the quantum resonance condition of the zero-point dipolar oscillations. This can be done if the nuclear spins become ordered as well, in a spatial configuration which has the same overall magnetic interaction energy with each of the two states of Fig. 1. We first note that the total on-site magnetic interaction is isotropic with respect to the direction of the nuclear spin. This is due to the simultaneous interaction of the nuclear spin with the zero-point electronic spin which has equal components oscillating along all 3 major axes.

The electric dipolar interactions in the ground-state of Fig.1 are such that each simple cubic sublattice of the bcc has no net interaction with the other sublattice. We therefore look for the possible static arrangements of the nuclear spins that fulfill the resonance requirement on each sublattice independently. Such arrangements are shown in Fig.6. In these arrangements there is an equal number of atoms with electronic and nuclear spins aligned (and anti-aligned) in both degenerate configurations of the electric dipoles (Fig.1). This arrangement also preserves the overall time-reversal symmetry of the system at zero field, i.e. no net magnetic polarization. Since these configurations exist on both sublattices, we end up with the u2d2 arrangements which is the symmetry of the ordered nuclear phase^{29,30}. The only constraint so far due to the quantum resonance is the u2d2-type symmetry (i.e. also u3d3 etc.). We would like now to describe in more detail the nature of the coherent state combining the zero-point electronic dipoles with the ordered nuclear spins.

The random on-site magnetic interaction can be thought of as a flipping of the dipoles with respect to the ground-state configuration of Fig.1. The average density, or probability, of a dipole-flip is given by the ratio of the magnetic energy E_{mag} to the electric dipole-flip excitation energy E_0 . The ground-state occupation of these flipped dipoles due to the magnetic interactions, means that there is a change in the zero-point occupation of the p electrons λ . The p -state mixing which is associated with these magnetically-induced flipped dipoles, is given by: $\lambda_m \sim \lambda \sqrt{E_{mag}/E_0} \simeq 10^{-2} \lambda$. This small polarization corresponds to an electric dipole moment: $\mu_m \simeq 10^{-2} \mu$, where μ is the full zero-point electric dipole moment (2). Since the magnetically-induced electric dipole-moments μ_m are interacting with each other, we are looking for configurations (of the type shown in Fig.6) that minimize this dipolar interaction energy (1) along the major axes (i.e. $\hat{\mu} = \hat{x}, \hat{y}, \hat{z}$)

$$E_{magdipole} = - \sum_{i \neq 0} \mu_{\mathbf{m},0} \cdot \mu_{\mathbf{m},i} \left[\frac{3 \cos^2(\hat{\mu}_{\mathbf{m}} \cdot (\mathbf{r}_0 - \mathbf{r}_i)) - 1}{|\mathbf{r}_0 - \mathbf{r}_i|^3} \right] \quad (7)$$

The configuration of Fig.6a has the lowest dipolar energy given by (7), and will therefore be chosen as the ground-state of the ordered phase. In this configuration,

the nuclear spins are aligned along a vector \mathbf{d} which is orthogonal to the u2d2 modulation axis \mathbf{l} (here along the (100) axis). One can see that the total dipolar interaction energy will be invariant under any rotation of the vector \mathbf{d} around \mathbf{l} . We therefore naturally obtain the state where the vector \mathbf{l} is along one of the major axes, as is found experimentally from the domain structure²⁹. We point-out that the u2d2 symmetry of the ordered phase results from symmetry and energy considerations which are independent of any quantitative parameters. This is in contrast to the MSE theory where the symmetry is determined by competition between many parameters^{1,4}.

In our picture, the interaction between the nuclear spins is indirect, being mediated by the electronic subsystem. This picture is somewhat similar to the hyperfine enhanced nuclear magnetism observed in certain insulators¹³. There, the nuclear polarization is effectively enhanced by an electronic spin that is partially aligned by a strong hyperfine interaction of a charged rare-earth ion. In our case, it is a quantum resonance of the electronic system that results in a coherent phase of oscillating electric and magnetic moments.

Experimentally, there is a marked difference between the hcp and bcc phases, in the sense that there is spin-ordering in the bcc phase, as opposed to the lack of such a transition in the hcp phase⁴⁶. This result is a natural consequence of our model, since we expect the triangular symmetry to frustrate any long-range dipolar ordering¹¹ of the type shown in Fig.1. Indeed there is no evidence for long-range zero-point electric dipole correlations in the hcp phase¹¹, in the form of large discrepancies between the SCH calculations of the phonon spectrum and the measured phonons. We therefore do not expect a priori any long-range ordering of the nuclear spins in the hcp phase³². In contrast, within the conventional MSE model, the absence of ordering of the spin system well below its Curie-Weiss temperature is not easily explained.

V. MAGNETIC EXCITATIONS AND ENERGY OF THE U2D2 PHASE

Due to the large ratio between E_0 and E_{mag} , the slow zero-point oscillations of the magnetically-excited electric dipoles μ_m can be decoupled from the much faster zero-point oscillation of the electric dipoles with natural frequency E_0/\hbar . The new coherent state can therefore be described as a tensor product of the coherent states of the two decoupled components of the oscillating electric dipoles. A fast component with natural frequency E_0/\hbar described by the Bose creation/annihilation operators a_k^\dagger, a_k representing approximately the full electric dipole moment (2), and a slow component described by the Bose creation/annihilation operators b_k^\dagger, b_k representing the electric dipole moment μ_m induced by the on-site hyperfine magnetic interaction. This decoupling of the magnetic and phononic quasi-particles is quite

natural¹, due to the difference of 3 orders of magnitude in the energy.

If we treat the magnetically-induced interactions as decoupled from the fast oscillating component, the total effective Hamiltonian for the new coherent state is

$$H = H_{phon} + H_{mag} \quad (8)$$

where H_{phon} is given in Eq.5 of Ref.^[11], and similarly

$$H_{mag} = \sum_k (2E_{magdipole} + X_{mag}(\mathbf{k})) b_k^\dagger b_k + \sum_k X_{mag}(\mathbf{k}) (b_k^\dagger b_{-k}^\dagger + b_k b_{-k}) \quad (9)$$

where b_k^\dagger, b_k are Bose creation/annihilation operators that represent a local flip of μ_m out of the ground-state (u2d2) arrangement, which behaves as a local-mode with bare energy (7) $E_{magdip} \equiv 2E_{magdipole} \simeq E_{mag}$, i.e. $X_{mag}(0) = -E_{magdip}/2$. The dipolar interaction $X_{mag}(\mathbf{k})$ is given by (7)¹¹

$$X_{mag}(\mathbf{k}) = - \sum_{i \neq 0} \mu_{\mathbf{m},0} \cdot \mu_{\mathbf{m},i} \left[\frac{3 \cos^2(\hat{\mu}_m \cdot (\mathbf{r}_0 - \mathbf{r}_i)) - 1}{|\mathbf{r}_0 - \mathbf{r}_i|^3} \right] \times \exp[2\pi i \mathbf{k} \cdot (\mathbf{r}_0 - \mathbf{r}_i)] \quad (10)$$

with \mathbf{k} being the wavevector characterizing the modulation of the array of the dipoles μ_m and nuclear spins, arranged in u2d2 configuration Fig.6a. Since the relative phase between the magnetically-induced electric dipole moments μ_m is determined by the relative alignment of the nuclear spins, there is a one-to-one correspondence between the modulation of the nuclear spins relative to the u2d2 arrangement, and modulation of the relative phase of the electric dipoles μ_m . The local-mode of energy E_{magdip} therefore corresponds also to a nuclear spin-flip out of the u2d2 ground-state arrangement.

The Hamiltonian H_{mag} (9) which describes the effective interaction between the magnetically induced dipoles μ_m can be diagonalized using the Bogoliubov transformation³³ $\beta_k = u(k)b_k + v(k)b_{-k}^\dagger$. The two functions $u(k)$ and $v(k)$ are given by: $u^2(k) = \frac{1}{2} \left(\frac{E_{magdip} + X_{mag}(k)}{E_{sw}(k)} + 1 \right)$, $v^2(k) = \frac{1}{2} \left(\frac{E_{magdip} + X_{mag}(k)}{E_{sw}(k)} - 1 \right)$, where the modulations of the magnetic Hamiltonian H_{mag} describe the energy spectrum of the spin-waves.

$$E_{sw}(k) = \sqrt{E_{magdip} (E_{magdip} + 2X_{mag}(k))} \quad (11)$$

The result of solving the effective Hamiltonian (9) is a coherent ground-state^{34,12}

$$|\Psi_0\rangle = \left(\prod_k \exp \left(\frac{v_k}{u_k} b_k^\dagger b_{-k}^\dagger \right) \right) |vac\rangle \quad (12)$$

A modulation of the relative phases of the magnetically-induced electric dipoles μ_m with a wavevector \mathbf{k} , represents a spin-wave since the nuclear spins have the same relative phase. We see that the electric dipolar interaction introduces an effective restoring force between the nuclear spins, that results in the above dispersion relation.

In Fig.7 we plot the dispersion relations of the spin waves obtained from Eq. (11), along various directions of the crystal. We find that the velocities of these waves at long wavelengths are in the range 6.0 – 10.0cm/sec (for $V \simeq 24\text{cm}^3/\text{mole}$). These values are similar to those extracted from melting pressure measurements³⁵, where a value of $8.4 \pm 0.4\text{cm/sec}$ was found. There is a soft excitation in the (100) direction ($c_{sw} \sim 3\text{cm/sec}$), and also an unstable excitation with an imaginary dispersion relation in the (010) direction, along which we therefore do not expect a propagating spin-wave. Along this direction the modulation in the nuclear spins breaks the quantum-resonance condition, which states that the total magnetic interaction energy is the same for both configurations of the dipoles of Fig.1. This modulation is therefore prohibited within the quantum resonance restriction. We note that this calculation was for the nuclear spins fully aligned with the z -axis.

Mean-field calculations of the MSE model³⁶ have also resulted in anisotropic spin-waves, though there is at present no experimental data on the directional anisotropy of the spin-waves to compare with theory.

In addition to Bosonic spin-waves there can also be local dipole-flips of the magnetically-induced electric dipoles μ_m . These π -shifted, i.e antisymmetric, dipole excitations are treated as Fermions, just as described previously for the full electric dipole moment¹². The energy spectrum of these excitations is given by¹²

$$E_{fm}(k) = \sqrt{E_{magdip}^2 + E_{sw}(k)^2} \quad (13)$$

The dispersion relation of these optic-like excitations is also plotted in Fig.7.

We can now calculate the contribution of all these excitations to the specific-heat. In the calculation, we included the individual contributions of each mode (in a spherical phase-space volume), and then simply averaged. Each type of excitation was treated with using the appropriate (Bose or Fermi) statistics, and the details are described in the Appendix (18). The agreement with the (limited) experimental data for the volume $V=24.13\text{cm}^3/\text{mole}$ ⁵ is fairly good (Fig.8). At this molar volume, we have $E_{magdip} \simeq 2.6\text{mK}$. We note that the contribution of the optic-like modes is important at higher temperatures, and that the agreement between the data and the simple T^3 law is somewhat fortuitous. Similar conclusions were reached using the MSE model³⁶. In particular, our calculation has the right slope as the experimental data.

For the specific volume $V \simeq 24\text{cm}^3/\text{mole}$, experimental data on the ground-state energy^{37,28} gives $E_{mag}/2 \sim$

$1.1 \pm 0.1\text{mK}$, while our calculation (4,5) gives $E_{mag}/2 \sim 1.3\text{mK}$. Plotting the free energies for the two phases (18),(16) in Fig.9, we find that they give a transition temperature: $T_N \sim 1.25\text{mK}$, close to the measured result³⁷ of $\sim 1.05\text{mK}$. In this calculation, we took the empirical value of $E_{mag}/2 = 1.1\text{mK}$, for the constant aligning energy appearing in (18),(16). In addition, the experimental data in Fig.9 was shifted up by 0.1mK, which is within the experimental uncertainty. We find that the flat free energy below the transition temperature fits the free energy of the ordered phase (18). It should be pointed out that this calculation, which is based on independent spin-waves, is valid only at low temperatures, compared to E_{mag} . We see that the energy difference between different spin arrangements which fit the symmetry constraint (such as u3d3 etc.¹), is only through the relatively small term ΔE_{dip} in the free-energy (17).

In Fig.10 we show the entropies of the two phases as a function of temperature, and indicate the jump at the approximate transition temperature. We obtain a latent heat of $\Delta ST_c \sim 100\mu\text{K}$ per atom, while experimentally it is found to be⁵ $\sim 250\mu\text{K}$ per atom. This degree of agreement is quite reasonable considering the crudeness of the spin-wave approximation at temperatures where the entropy is already $\sim 0.35 \ln(2)$, and the independent spin-wave picture is questionable.

Finally we describe the magnetic response of the u2d2 phase. The zero-temperature susceptibility of an antiferromagnet with the field orthogonal to the magnetic moments³⁸, is given by: $\chi(0) = \mu_n^2/E_{mag}$, where $E_{mag}/2$ is the aligning energy, and we use the effective nuclear moment, reduced by a factor of 0.83, due to the quantum fluctuations⁵. The calculated susceptibility is smaller by $\sim 15\%$ than the measured value³⁹, and is therefore in reasonable agreement.

The zero-field antiferromagnetic resonance frequency², measured by NMR²⁹, is given by: $\hbar^2 \Omega_0^2 = 4E_d E_{mag}$, where E_d is the direct nuclear magnetic dipolar interaction. To calculate the temperature dependence of this quantity, we calculate (Appendix) the reduction in the ordered magnetic moment due to thermal occupation of excited states¹. Since E_d depends on the ordered nuclear magnetic moment N_n squared, we have that $\Omega_0 \propto N_n$. In Fig.11 we plot the normalized temperature dependence of Ω_0 compared to the thermally reduced magnetic moment: $(1 - \Delta M)$ (Eq.(19)). We find that the reduction in the frequency is well described by our calculation, up to $\sim 0.7\text{mK}$, above which the experimental data have a steeper decline. We further note that NMR experiments measure the resonance of the stationary nuclear spin, and do not reflect the fast-oscillating ($\omega = E_0/\hbar$) zero-point electronic magnetic moments \mathbf{N}_e .

Our final comment about the u2d2 phase is concerning its domain structure. It was found^{40,41} that a crystal grown in a narrow channel will have one large magnetic domain which will be oriented such that the magnetic planes are parallel with the channel axis and surface. This observation can be explained by our model in the

following way. On the channel surface the coherent motion of the atoms is inhibited in the direction normal to the wall. The only remaining coherent motion is parallel to the wall surface, and so will therefore be the magnetic ordering. At the nucleation site, when the crystal grows into the free liquid, it will have the three domains along the three orthogonal major axes. The relative sizes of the domains will be determined by random roughness at the nucleation site⁴¹.

VI. HIGH-FIELD PHASE

Above a critical external magnetic field H_{c1} there is a first-order transition to a high-field phase (HFP). The NMR data for this phase⁴² indicates a phase with cubic symmetry and large magnetization: $N_z > 0.6$ (in units of the saturation magnetization³⁹). The nuclear spin arrangement inferred for this phase is shown in Fig.12. Since there is now global nuclear magnetization along the field direction (z -axis in Fig.13), there is no time reversal symmetry and no quantum resonance, for the oscillating electric dipole moments μ_m along this axis. Along the orthogonal xy -directions there is still quantum resonance for the electronic dipoles μ_m 's, and hyperfine interactions of energy E_{mag} . In a semi-classical picture, the nuclear spins are vectors with the magnetization in the z -direction given by their z -component, precessing around the z -axis with the Larmor frequency. In the paramagnetic-phase (PP) the xy -components of the spins are random, while in the HFP there is long-range order for these components (Fig.13), due to the aligning effect of the hyperfine interactions in the xy -plane. The order-parameter is therefore the global phase of the coherent xy -components μ_m^{xy} , i.e. a complex order-parameter, and we expect a second-order phase transition of the type found for example in superfluid ^4He , which is also in the 3D-XY universality class⁴³. Further, the specific-heat data⁵ of the HFP has a distinct cusp at the transition temperature, typical of a λ -type transition.

Let us examine the field dependence of the hyperfine magnetic interactions in the xy -plane, by first looking at the electronic polarization. With increasing external magnetic field the electronic spins \mathbf{N}_e in the xy -plane will become oriented with the external field along the z -direction, reducing the hyperfine interactions with the nuclear spins in the xy -directions (4). The electronic spins are oriented with the oscillating p -states of the atom in the xy plane, with effective energy $\langle E_{es} \rangle \sim 1.4(1 - F)\text{K}$, where the factor $1 - F$ takes into account the overlap of the different electronic spin orientations (5, Fig.3), reducing the effective energy gap. The single-atom magnetic Hamiltonian for the electronic spins in the xy -plane, in an external field H is therefore

$$H_{elec} \simeq -\frac{1}{2}E_{es}N_e^{x2} - HN_e^z \quad (14)$$

with N_e^x, N_e^z the classical components of \mathbf{N}_e . The first term represents the aligning dipolar interaction between the s and p electrons of the atom. Solving (14) by mean-field, we get a linear magnetization: $N_e^z = H/E_{es}$, and full magnetization of the electronic spins \mathbf{N}_e at a field: $H_{c2} \sim 26\text{T}$ (using $(1 - F) \sim 0.6$ for $V \sim 24\text{cm}^3$, so that $E_{es}/2 \sim 0.4\text{K}$), in rough agreement with the estimated^{39,9} experimental value of $\sim 22\text{T}$. At fields larger than H_{c2} there are no xy hyperfine interactions so the nuclear spins are free to fully align with the external field, and there is a zero-temperature transition to the PP.

The volume dependence of H_{c2} is experimentally⁴⁴ found to have a volume dependence which is steeper than the critical Neel temperature T_N of the u2d2 phase. This is in agreement with our formulation (14), as H_{c2} is given by the steep dependence of the factor $(1 - F)$ (Fig.5). Since T_N is roughly proportional to E_{mag} (Fig.9), we get: $\frac{H_{c2}(V_1)}{H_{c2}(V_2)} \frac{\lambda(V_1)}{\lambda(V_2)} \simeq \frac{T_N(V_1)}{T_N(V_2)}$ (using Eqs.4,5 and $\lambda(V)$ from Fig.2a). Comparing the data^{39,28,44} at $V_2=24\text{ cm}^3/\text{mole}$ and $V_1=22.7\text{ cm}^3/\text{mole}$ we find: $\frac{H_{c2}(V_1)}{H_{c2}(V_2)} \sim 0.25$, $\frac{\lambda(V_1)}{\lambda(V_2)} \sim 1.2$ and $\frac{T_N(V_1)}{T_N(V_2)} \sim 0.3$, in excellent agreement with the above relation.

If the electronic spins μ_m in the xy -plane would have an arrangement where the dipolar interaction energy is negative (such as the u2d2 phase (7)), they would have zero-point oscillations with the resulting dipolar interaction energy E_{magdip} (9,10). These oscillations would get them out of phase with the nuclear spins, which are precessing with the Larmor frequency. We therefore can only have a cubic arrangement with zero ground-state dipolar interactions. In Fig.13 we plot the dipolar interaction energy X_{hfp} (10) of the xy -components μ_m^{xy} as a function of modulation wavevector k along the (001)-axis, with respect to the ground-state array of Fig.13. We find that the dipolar interaction energy is indeed zero in the ground-state, with a quadratic dispersion similar to excitations in a ferromagnet.

We shall now describe the nuclear spins in the HFP. In the HFP the nuclear spins will have a stiffness against small perturbation from the ordered configuration of Fig.13 (see Fig.13). Perturbations of the nuclear spins in the xy -plane will cost an energy X_{hfp} (Fig.13), while the z -component perturbation costs the Zeeman energy $E_{zeeman} = N_n H$. A simple description of this state is therefore by the following model magnetic Hamiltonian of independent nuclei

$$H_{hfp} \simeq -H\sigma_z N_n^z - E_x \sigma_x N_n^x \quad (15)$$

where H is the external field in units of energy, $E_x = E_{mag}/2$ is the effective aligning energy of the xy -components compared with the random arrangement of the nuclear spins (see Eq.16), N_n^z, N_n^x are the components of the nuclear spin. The size of the hyperfine xy -interactions of the nuclear spins with the electronic spins will be reduced with increasing magnetic field:

$$E_x \propto \mathbf{N}_e^x \simeq \sqrt{1 - H/H_{c2}} \quad (4,14).$$

The energy of the nuclear spin is therefore given by $E_{hfp} = -\sqrt{H^2 + E_x^2}$. We plot in Fig.14 the energy E_{hfp} compared with the energy of the u2d2 phase at zero temperature (18): $E_{u2d2} = -(E_{mag}/2) - \Delta E_{dip} - \chi(0)H^2$ (using at $V=24\text{cm}^3$ $E_{mag}/2 \sim 1.1\text{mk}$, see Sec. V). We see that the HFP has lower energy than the u2d2 phase at fields $H > 0.7\text{T}$, which is quite close to the measured value^{39,9} of $H_{c1} \sim 0.45\text{T}$. In Fig.14 we also plot the magnetization of the u2d2 phase: $N_{u2d2} = \chi(0)H$, compared with the measured magnetization^{39,9}, and as calculated for the HFP (15): $N_{hfp} = -2H(H + E_{hfp})/E_x^2$. We find that the calculated magnetization is ~ 0.55 at the calculated critical field H_{c1} , which is close to the measured value^{39,9} of ~ 0.6 .

We further checked the dependence of this critical field on the magnetic energy E_{mag} , and we find that it has a weaker than linear dependence, in accordance with the experimental data²⁸. Taking $E_{mag} \propto T_N$ and using the measured²⁸ values at $V_1 = 24.21\text{cm}^3$ and $V_2 = 22.45\text{cm}^3$, we calculate a ratio of critical fields of $H_{c1}(V_1)/H_{c1}(V_2) \sim 3.4$, compared to the measured ratio of ~ 3 (while the transition temperatures vary by a factor of ~ 4.2).

We note that our description of the HFP is at best qualitative, since at higher magnetic fields the calculated magnetization N_{hfp} is much larger than the measured magnetization (Fig.15). Using the measured magnetization we shall now use (15) to describe the phase diagram of the HFP. The overall stiffness of the spins should be proportional to the transition temperature of HFP to PP, since the stiffness represents the energy cost to randomize the spins and create a PP. From (15) and Fig.13 this energy should be given by the geometric-mean of the energies appearing in (15): $E_{mean} = \sqrt{(HN_z)(E_x N_x)}$, where N_z is the measured magnetization (Fig.15) and $N_x = \sqrt{1 - N_z^2}$. We find that a constant factor of ~ 1.3 relates this last expression (E_{mean}) with T_c , and is in excellent agreement with the measured T_c (Fig.16).

VII. CONCLUSION

To conclude, our model enables us to describe both the phonon spectra and the nuclear magnetic ordering of bcc ^3He using a single parameter, which is the thermal activation energy E_0 . The model offers a consistent picture of the nature of the magnetic phases of bcc ^3He , and their phase diagram. We give a quantitative description of the u2d2 phase, which compares well with the measured data. Despite the more qualitative nature of our description of the HFP, we obtain a good description of the phase diagram parameters: H_{c1}, H_{c2}, T_c and their field and volume dependence.

We are currently exploring the consequences of this model regarding the description of the magnetic properties of solid ^3He in confined geometries (nano-clusters,

aerogel) and in lower dimensions such as adsorbed two-dimensional films.

Acknowledgements N.G. thanks Tony Leggett and Gordon Baym for many useful discussions and suggestions. This work was supported by the Israel Science Foundation, the Technion VPR fund for the Promotion of Research, the Fulbright Foreign Scholarship grant, NSF grant no. DMR-99-86199 and NSF grant no. PHY-98-00978.

VIII. APPENDIX

Here, we present details of the calculation of the free-energy and magnetization of the u2d2 phase.

The ground-state energy of the nuclear spins has two contributions. The first is the reduction of energy compared to the random case, where the electronic dipoles μ_m of everage energy $E_{mag}/2$ are excited. This energy is equivalent to an effective magnetic field that tends to align the nuclear spins, and its effects already appear significant in the PP. The free energy of the PP, can be therefore written as⁴⁵

$$F_{para} \simeq -k_B T \ln [2 \cosh(E_{mag}/2k_B T)] \quad (16)$$

In the ordered, coherent u2d2 phase, there is an additional reduction in the ground-state energy of the coherent magnetically-induced electric dipoles μ_m due to their negative dipolar interaction^{33,12}

$$\begin{aligned} \Delta E_{dip} &= \sum_k \frac{E_{sw}(k) - (E_{magdip} + X_{mag}(k))}{2} \\ &\simeq -50\mu K/atom \end{aligned} \quad (17)$$

where we again calculated the contribution from each Bosonic mode and then averaged. In the u2d2 phase there are therefore coherent zero-point electronic dipoles μ_m , which reduce the ground-state energy (12), oscillating with a resonance energy E_{magdip} (9,10). The free energy of the ordered phase can therefore be approximated as

$$\begin{aligned} F_{u2d2} &\simeq \Delta E_{dip} - (E_{mag}/2) \\ &+ k_B T \left[\sum_k \ln(1 - \exp(-E_{sw}(k)/k_B T)) \right. \\ &\quad \left. - \sum_k \ln(1 + \exp(-E_{fm}(k)/k_B T)) \right] \end{aligned} \quad (18)$$

The specific-heat $C_v = -T\partial^2 F/\partial T^2$ and entropy $S = \partial F/\partial T$ are then calculated from these free energies.

We now calculate the reduction in the ordered magnetic moment due to thermal occupation of excited states¹. For the Bosonic and Fermionic excitations (11,13) we have a reduction in magnetization which is proportional to the occupation of excited states

$$\Delta M = \sum_k [u_k^2 n_B + v_k^2 (1 - n_B)] - \sum_k [w_k^2 n_F + y_k^2 (1 + n_F)] \quad (19)$$

where n_B, n_F are the Bose/Fermi occupation factors respectively, and $(u_k, v_k), (w_k, y_k)$ are the Bose and Fermi Bogoliubov factors¹². The factors (u_k, v_k) were given before (section V), while the Fermi factors are given by¹²

$$w_k^2 = \frac{1}{2} \left(1 + \frac{E_{magdip}}{E_{fm}(k)} \right), y_k^2 = \frac{1}{2} \left(1 - \frac{E_{magdip}}{E_{fm}(k)} \right) \quad (20)$$

-
- ¹ M. Cross and D. Fisher, *Rev. Mod. Phys.* **57** (1985) 881.
² M. Cross, *Jap. J. of App. Phys.* **26** (1987) 1855.
³ W.P. Halperin, F.B. Rasmussen, C.N. Archie and R.C. Richardson, *J. Low Temp. Phys.* **31** (1978) 617.
⁴ M. Roger, J.H. Hetherington and J.M. Delrieu, *Rev. Mod. Phys.* **55** (1983) 1.
⁵ D.S. Greywall and P.A. Busch, *Phys. Rev. B* **36** (1987) 6853.
⁶ D.M. Ceperley and G. Jacucci, *Phys. Rev. Lett.* **58** (1987) 1648.
⁷ B. Cowan and M. Fardis, *Low Temp. Phys.* **23** (1997) 448.
⁸ J. DuBois and P. Kumar, *J. Low Temp. Phys.* **98** (1995) 37.
⁹ D.D. Osheroff and H. Godfrin, *Phys. Rev. B* **38** (1988) 4492.
¹⁰ N. Gov and E. Polturak, QFS2000 conference, to appear in *J. Low Temp. Phys.*
¹¹ N. Gov and E. Polturak, *Phys. Rev. B* **60** (1999) 1019.
¹² N. Gov, *Phys. Rev. B* (2000) **62** (2000) 910.
¹³ Y. Masuda and H. Suzuki, *J. Low Temp. Phys.* **75** (1989) 159.
¹⁴ H.R. Glyde, 'Excitations in Liquid and Solid Helium', Oxford Series on Neutron Scattering in Condensed Matter, 1994.
¹⁵ L.H. Nosanow *Phys. Rev.* **146** (1966) 120.
¹⁶ I.B. Bersuker and V.Z. Polinger, 'Vibronic Interactions in Molecules and Crystals', 1983, Springer Series in Chemical Physics 49.
¹⁷ C.A. Burns and J.M. Goodkind *J. Low Temp. Phys.* **95** (1994) 695.
¹⁸ D.S. Greywall, *Phys. Rev. A* **3** (1971) 2106.
¹⁹ T.R. Kohler, *Phys. Rev. Lett.* **18** (1967) 654.
²⁰ S.M. Heald, D.R. Baer and R.O. Simmons, *Phys. Rev. B* **30** (1984) 2531.
²¹ D.S. Greywall, *Phys. Rev. B* **15** (1977) 2604.
²² I. Iwasa and H. Suzuki, *J. Low Temp. Phys.* **62** (1986) 1.
²³ C. Seyfert, R.O. Simmons, H. Sinn, D.A. Arns and E. Burkel *J. Phys.: Condens. Matter* **11** (1999) 3501.
²⁴ Cohen Tanoudji, 'Quantum Mechanics', Vol. II, Wiley-Interscience (1977).
²⁵ R.F. Bishop *et. al.*, cond-mat/0011008.

- ²⁶ W. Vassen and W. Hogervorst, *Phys. Rev. A* **39** (1989) 4615.
²⁷ N.W. Ashcroft and N.D. Mermin, 'Solid State Physics', Saunders College Publishing, 1976.
²⁸ H. Fukuyama *et. al.*, *Phys. Rev. Lett.* **67** (1991) 1274.
²⁹ D.D. Osheroff, M.C. Cross and D.S. Fisher, *Phys. Rev. Lett.* **44** (1980) 792.
³⁰ A. Benoit, J. Bossy, J. Flouquet and J. Schweizer, *J. Phys. Lett.* **46** (1985) L923.
³¹ T. Okamoto *et. al.*, *Phys. Rev. Lett.* **71** (1994) 868.
³² The measured ferromagnetic short-range correlations^{46,47} in the hcp phase can result from nearest-neighbor (i.e. local) dynamical correlations. Local correlations of the zero-point motion will result in electronic polarization and hyperfine interactions similar in size to those calculated for the bcc. These may cause the observed local (i.e. randomly oriented) ferromagnetic correlations.
³³ P.W. Anderson, 'Concepts In Solids', 1963, p.132-148.
³⁴ K. Huang, 'Statistical Mechanics', 1987, John Wiley and Sons, Inc..
³⁵ D.D. Osheroff and C. Yu, *Phys. Lett.* **77A** (1980) 458.
³⁶ Z. Sun and J.H. Hetherington, *J. Low Temp. Phys.* **91** (1993) 299.
³⁷ H. Fukuyama *et. al.*, *Phys. Rev. B* **36** (1987) 8921.
³⁸ Kittel, 'Introduction to Solid State Physics'.
³⁹ D.D. Osheroff, H. Godfrin and R. Ruel, *Phys. Rev. Lett.* **58** (1987) 2458.
⁴⁰ Y.P. Feng, P. Schiffer, J. Mihalisin and D.D. Osheroff, *Phys. Rev. Lett.* **65** (1990) 1450.
⁴¹ Y. Sasaki, T. Matsushita, T. Mizusaki and A. Hirai, *Phys. Rev. B* **44** (1991) 7362.
⁴² D.D. Osheroff, *Physica B* **109,110** (1982) 1461.
⁴³ C. Domb and M.S. Green, 'Phase Transitions and Critical Phenomena', Vol.3, p. 570, London, New York, Academic Press (1974).
⁴⁴ H. Fukuyama *et. al.*, *Physica B* **169** (1991) 197.
⁴⁵ R.K. Patria, 'Statistical Mechanics', 1984, Pergamon Press Ltd., Oxford, England.
⁴⁶ T. Okamoto *et. al.*, *Phys. Rev. Lett.* **71** (1994) 868.
⁴⁷ T. Lang *et. al.*, *Phys. Rev. Lett.* **77** (1996) 322.

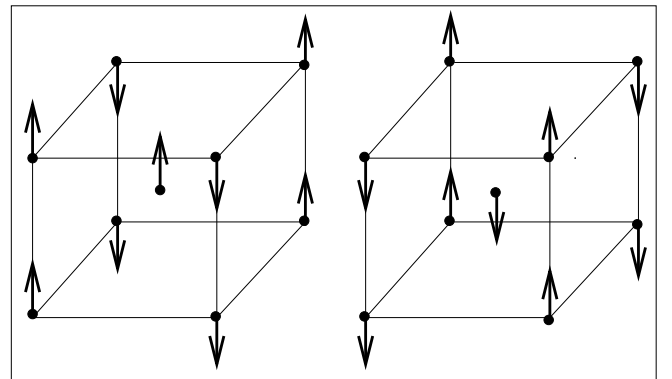


FIG. 1. The two degenerate 'antiferroelectric' dipole arrangement in the ground-state of the bcc phase. The arrows show the instantaneous direction of the dipoles.

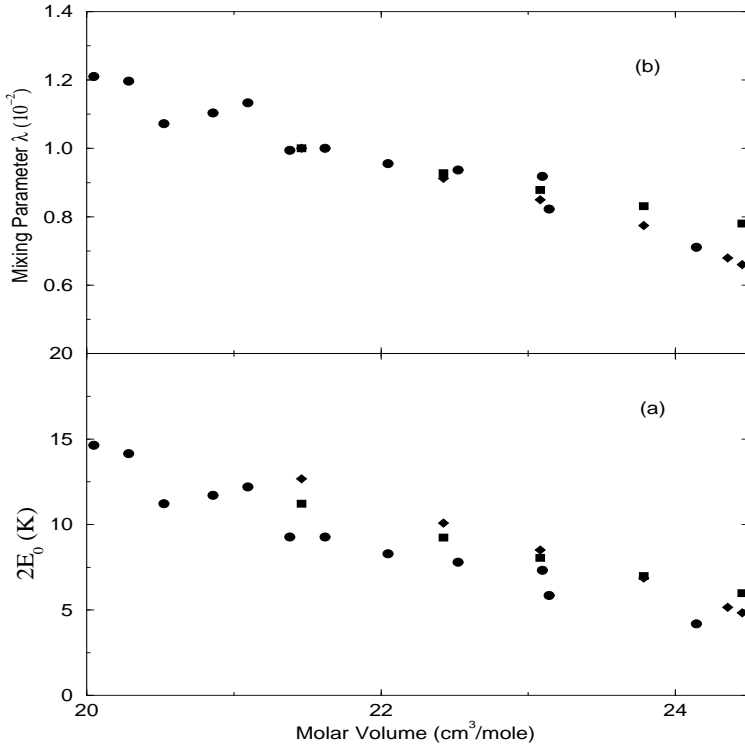


FIG. 2. (a) The dipolar activation energy $2E_0$ from experimental data: Circles²⁰, squares²¹ and diamonds²². (b) The mixing parameter λ (Eq.2) from the experimental data of (a).

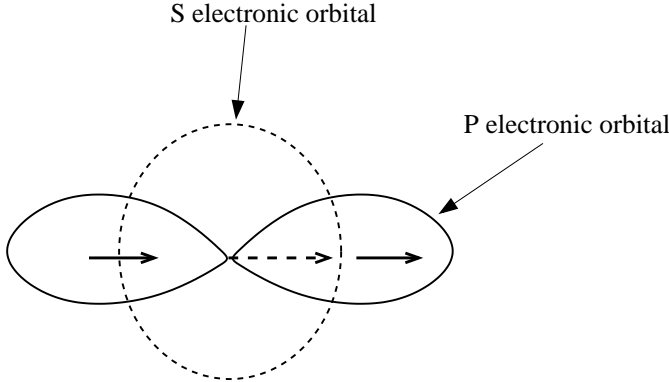


FIG. 3. The spin-orbit electronic magnetic-dipole interaction E_{es} which aligns the s -shell spin in the center (dashed arrow) with the p -shell spin in the lobes (solid arrows).

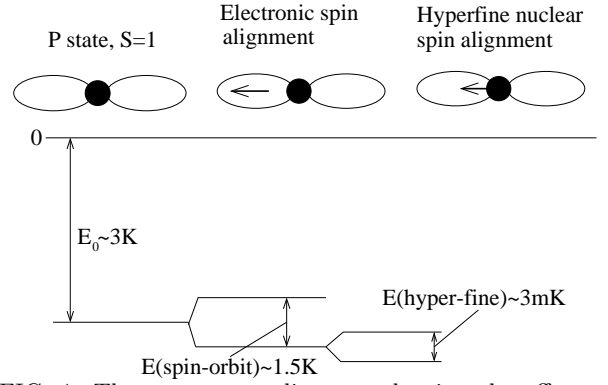


FIG. 4. The energy tree-diagram, showing the effects on the electronic and nuclear subsystems due to the coherent zero-point dipoles. The first effect is the excitation of λ p -state with $S = 1$, with energy E_0 . The second effect is the alignment of the electronic spins with the electric dipole (E_{es}). The last effect is the hyperfine interaction that aligns the nuclear spin with the electronic spin with energy E_{mag} (Eq.4).

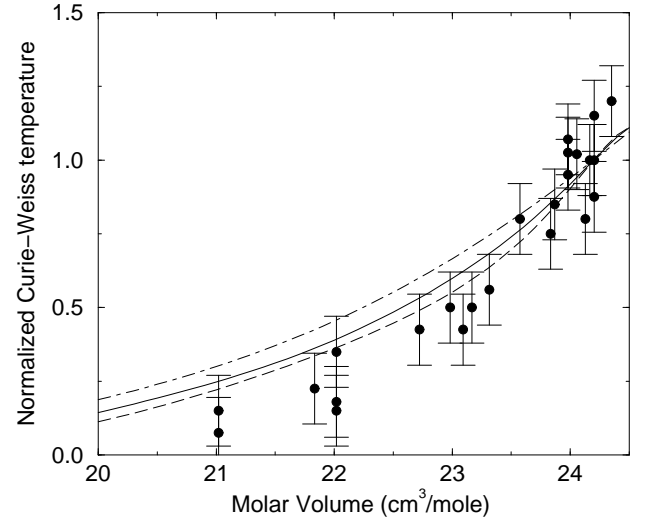


FIG. 5. The normalized magnetic splitting $2E_{mag}$ (Eq.4) as a function of volume, calculated using different experimental data sets for the activation energy E_0 : dashed line²⁰, dash-dot²¹ and solid line²². The solid circles are the normalized experimental Curie-Weiss temperature θ^1 .

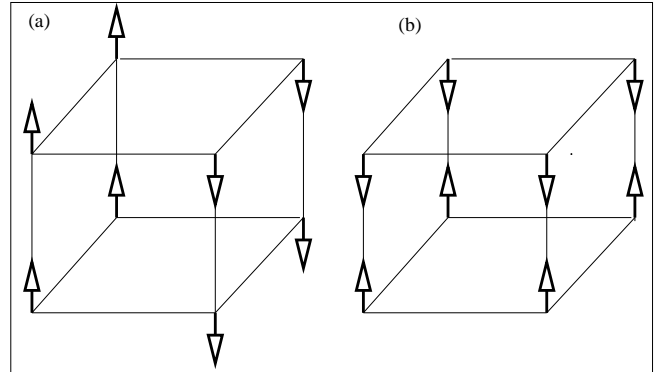


FIG. 6. Example of two simple u2d2 static nuclear spin (arrows) arrangements that maintain the quantum resonance of both the electric and magnetic dipoles (Fig.1). Only the spins on one simple-cubic sublattice of the bcc are shown, with the other sublattice having identical arrangement.

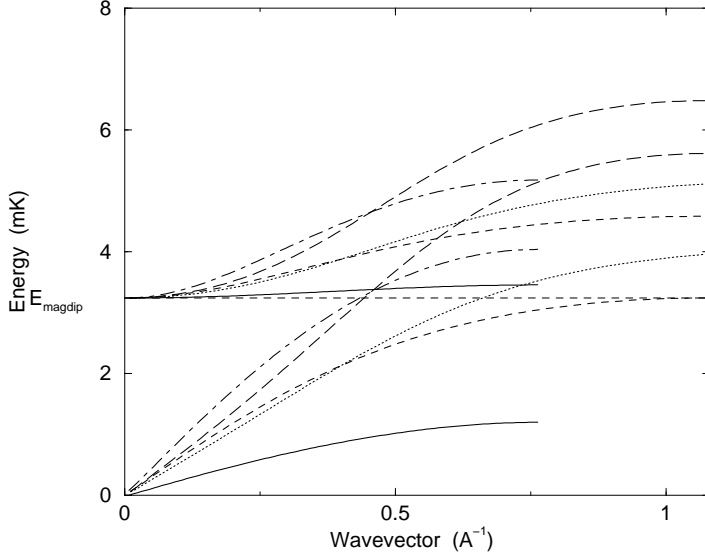


FIG. 7. The spin-wave spectrum $E_{sw}(k)$ (Eq.11) and the optic-like branches of the fermionic excitations $E_{fm}(k)$ (Eq.13). The nuclear spins are arranged as shown in Fig.6a, and the excitations are long the directions: (100)-solid, (101)-long dashed, (001) dash-dot, (011)-dashed, (111)-dotted.

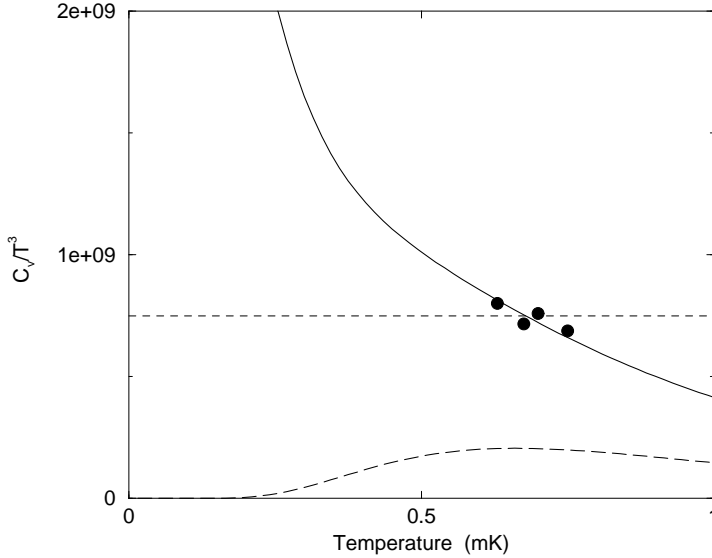


FIG. 8. The calculated total specific-heat (from Eq.18) (solid line), compared to experimental results⁵ at $V = 24.13 \text{ cm}^3/\text{mole}$ (solid circles). We also plot the contribution of the fermionic modes (heavy dashed-line), and the linear spin-wave approximation (thin dashed line). In this calculation we used $E_{mag} = 2.6 \text{ mK}$.

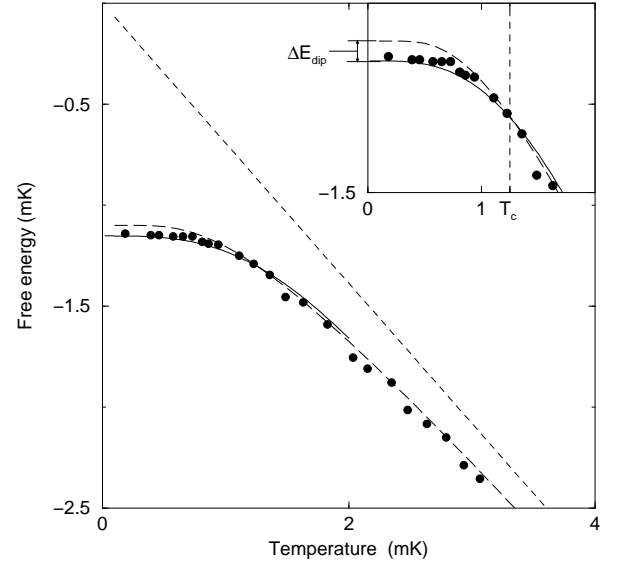


FIG. 9. The calculated free energies of the coherent u2d2 magnetic dipoles (solid line, Eq.18), of the PP (dashed line, Eq.16), of free spins (thin dashed line) and the experimental data³⁷ (solid circles). The inset shows the transition region.

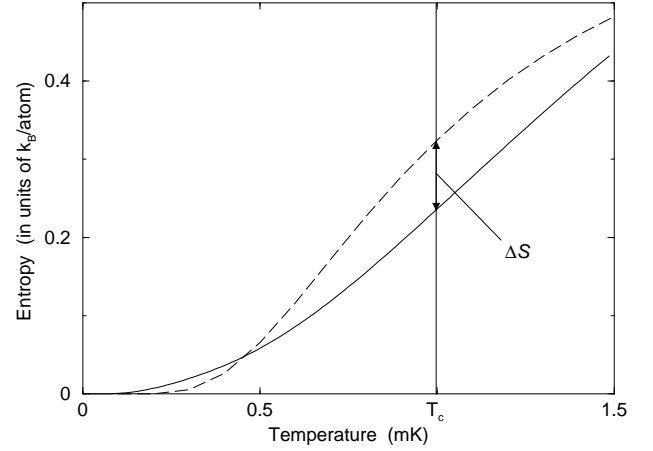


FIG. 10. The calculated entropies of the ordered phase (solid line) and of the PP (dashed-line). At the approximate transition temperature of 1mK we show the jump in entropy which gives a latent heat at the first-order transition of $\sim 100 \mu\text{K}$ per atom.

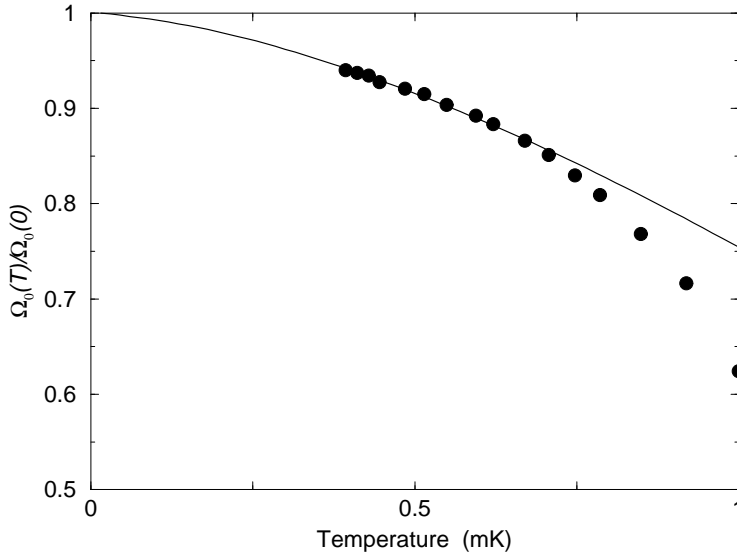


FIG. 11. The temperature dependence of the calculated ordered nuclear magnetic moment (Eq.19) compared with the measured²⁹ normalized antiferromagnetic resonance frequency Ω_0 .

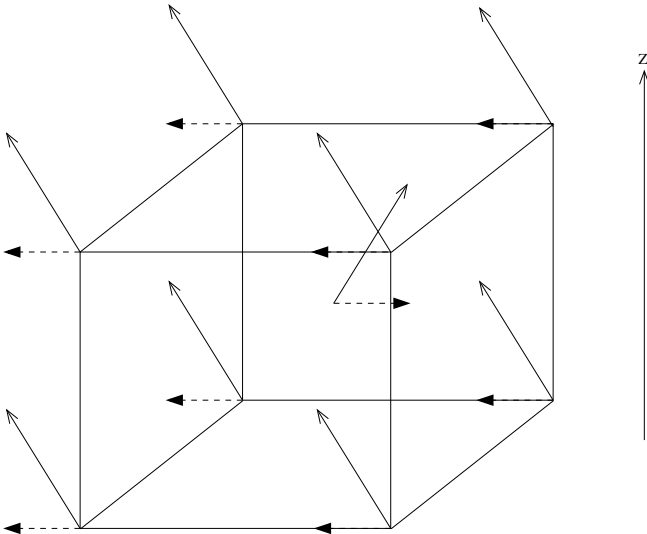


FIG. 12. The High-Field Phase (HFP) arrangement of the nuclear spins. A ferromagnetic arrangement in each sublattice of the xy -component (dashed arrows), with zero total xy magnetization. The external field B is in the z -direction.

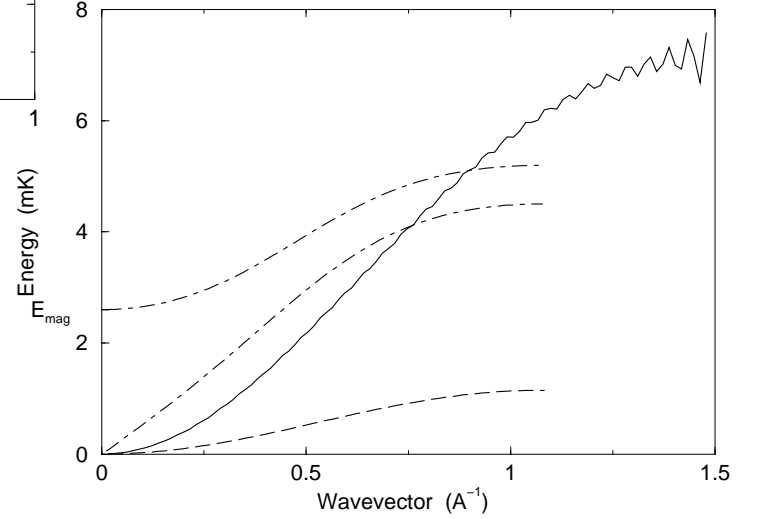
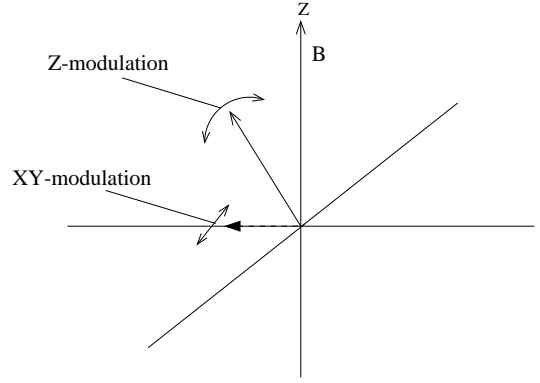


FIG. 13. (a) Schematic description of the small spin perturbations of the xy and z components. (b) The dipolar interaction matrix $X_{hfp}(k)$ between the xy electronic dipoles μ_m , as a function of the wavevector in the (001)-direction (solid line), (101)-direction (dashed line) and typical spin-waves of the u2d2 phase (dash-dot lines).

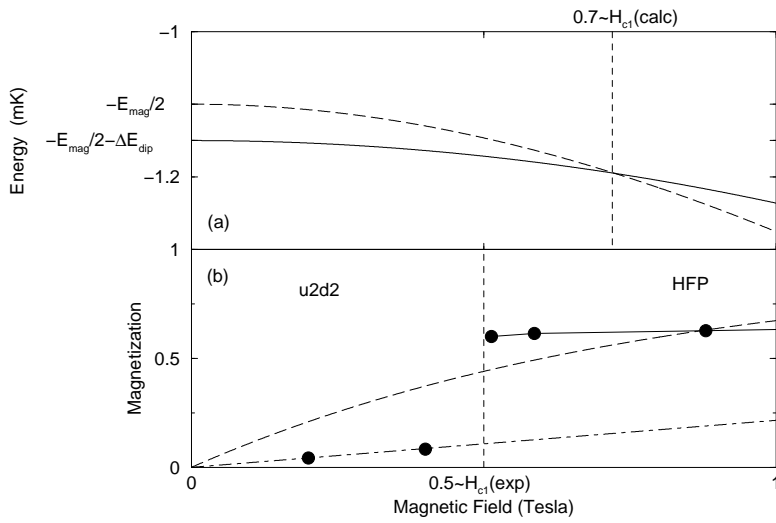


FIG. 14. (a) Comparison between the calculated zero-temperature energies of the u2d2 phase (E_{u2d2} Eq.18, solid line), HFP (E_{hfp} Eq.15, dashed line) as a function of magnetic field. The calculated transition at $H_{c1} \simeq 0.7$ T. (b) Comparison between the calculated zero-temperature magnetization of the u2d2 phase (N_{u2d2} , dash-dot line), HFP (N_{hfp} , dashed line) and the experimental data³⁹ (solid circles with guiding solid line). The measured transition is at $H_{c1}(exp) \sim 0.5$ T.

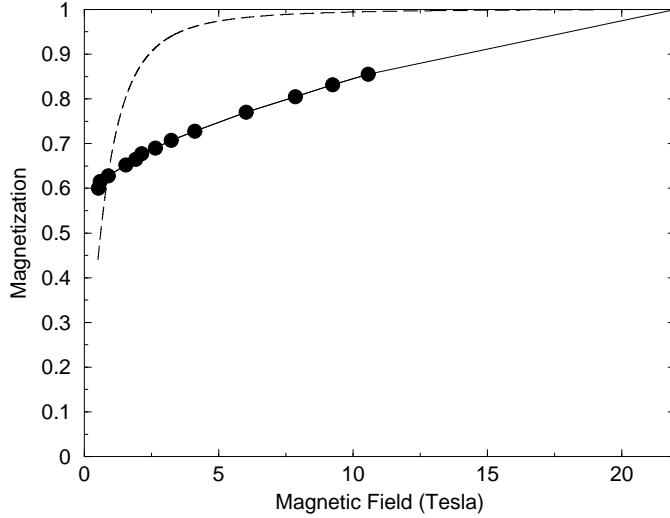


FIG. 15. Comparison between the calculated zero-temperature magnetization of the HFP (N_{hfp} , dashed line) and the experimental data³⁹ (solid circles with solid line).

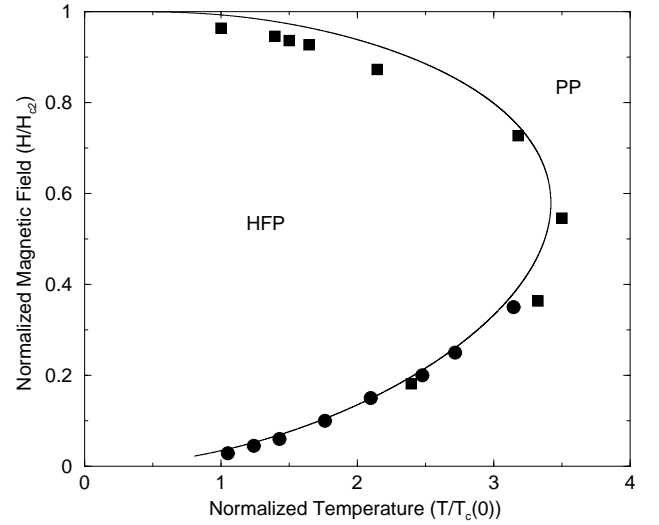


FIG. 16. The geometric-mean energy $E_{mean} \times 1.3$ (solid line) compared with the normalized transition temperature $T/T_c(0)$ (solid circles⁵, solid squares⁴⁴) as a function of normalized magnetic field H/H_{c2} .